Atmos. Chem. Phys. Discuss., 10, 22469–22513, 2010
www.atmos-chem-phys-discuss.net/10/22469/2010/
doi:10.5194/acpd-10-22469-2010

Atmospheric Chemistry and Physics Discussions

Aerosol flux measurements above a mixed forest at Borden, Ontario

M. Gordon, R. M. Staebler, J. Liggio, A. Vlasenko, S.-M. Li, and K. Hayden

Science and Technology Branch, Environment Canada, Toronto, Canada

Received: 16 July 2010 – Accepted: 20 September 2010 – Published: 1 October 2010

Correspondence to: M. Gordon (mark.gordon@ec.gc.ca)

Published by Copernicus Publications on behalf of the European Geosciences Union.

Abstract

Aerosol fluxes were measured above a mixed forest by Eddy Covariance (EC) with a Fast Mobility Particle Sizer (FMPS) at the Borden Forest Research Station in Ontario, Canada between 13 July and 12 August 2009. The FMPS, mounted at a height of 33 m (approximately 10 m above the canopy top) and housed in a temperature controlled enclosure, measured size-resolved particle concentrations for 3 to 410 nm at a rate of 1 Hz. For the size range $20<D<410$ nm, 60% of fluxes were upward. The exchange velocity is between -0.5 and 2.0 mm s^{-1}, with median values near 0.5 mm s^{-1} for all sizes between 24 and 280 nm. The net production rate of particles is highest for 75 nm particles and is near 0.4×10^{6} m^{-2} s^{-1}. Results indicate a decoupling of the above and below canopy spaces, whereby particles are stored in the canopy space at night, and are then diluted with cleaner air above during the day. Chemically speciated flux measurements from a previous study at the same location using a Quadrupole Aerosol Mass Spectrometer (Q-AMS) demonstrate a tendency towards downward fluxes, which may be due to an organic particle component which can not be resolved by the flux mode of the Q-AMS.

1 Introduction

Atmospheric aerosol particles are generated by both anthropogenic and natural sources and through chemical and physical processes in the atmosphere. The sizes of airborne aerosols range from nm to tens of µm. The dynamics of atmospheric aerosols is highly complex, involving particle formation, growth, and surface exchange processes. Effects of aerosols include direct and indirect climate forcing (IPCC, 2007) through the absorption and scattering of incoming solar radiation and the formation of clouds by condensation nuclei activation; reduction of visibility (Malm, 2003); and impairment to human health (Lippmann, 2009). Aerosols are carriers of compounds containing nitrogen (N), sulphur (S), and other elements over large distances. The eventual

ACPD
10, 22469–22513, 2010

deposition of nitrate (NO_3^-) and sulphate (SO_4^{2-}) aerosols can lead to acidification and eutrophication of the environment, especially in sensitive ecosystems (Spranger et al., 2004).

Dry deposition of aerosols to the surface is primarily a function of particle size, boundary layer conditions (turbulence intensity), and collecting properties of the surface. The theoretically predicted deposition rate is lowest for particle sizes between 100 nm and 2 µm, with several orders of magnitude difference between different models (cf. Petroff et al., 2008). In a review of particle atmosphere-surface exchange, Pryor et al. (2008b) conclude that: few studies have sought to quantify the dependence of flux on particle size; observations over forests do not support the theoretical minimum depositions rate manifest in models; and that more research is required to determine if dry deposition of aerosols is an important removal mechanism for ultrafine particles, especially over surfaces with high roughness, such as forests. There have been a number of studies which have measured size-resolved aerosol fluxes over forests. Forest types and locations include: mixed deciduous in Southern Indiana, USA (Pryor et al., 2009); pine in Hyytiälä, Finland (e.g., Buzorius et al., 1998, 2000, 2001; Gronholm et al., 2007); maritime pine in Les Landes, France (Lamaud et al., 1994); spruce in Germany, at Solling (Bleyl, 2001) and near Münchberg (Held and Klemm, 2006); beech in Soro, Denmark (Pryor, 2006); and Amazonian rain forest near Manaus, Brazil (Ahlm et al., 2009). The majority of these studies measured aerosol fluxes using the eddy covariance (EC) technique with Condensational Particle Counters (CPCs), which measure the total particle number concentration over a particle size range typically between 10 nm and 1 µm. Recently, size-resolved fluxes have been measured, using Relaxed Eddy Accumulation (REA) with a Differential Mobility Particle Sizer (DMPS; Gronholm et al., 2007), and EC with a Fast Mobility Particle Sizer (FMPS; Pryor et al., 2009).

Lamaud et al. (1994) found that particle deposition velocity (V_d) is related to friction velocity (u_*) and atmospheric stability. This was also supported by the studies of Gronholm et al. (2007), Pryor (2006), Pryor et al. (2007), and Ahlm et al. (2009). Many

ACPD
10, 22469–22513, 2010

studies found fluxes were often upward (negative "deposition"), with frequency ranging from near 20% (Gronholm et al., 2007) to over 40% (Pryor et al., 2008c) of the total number of flux measurements. Upward fluxes have been attributed to local emissions (Buzorious et al., 2000), sources of particles within or close to the canopy top (Buzorius et al., 1998), stochastic effects in the data (Gaman et al., 2004), and entrainment during the growth of the mixing layer (Nilsson et al., 2001). Pryor et al. (2008a) analysed data from two locations with the aim of determining the source of these upward fluxes. They found a possible causal link of upward fluxes to the entrainment of particle-depleted air from the free troposphere at one location. However, no such link was apparent at the second location. They concluded that further research is warranted.

The following describes a study which took place in a mixed coniferous and deciduous forest at the Borden Forest Flux Tower between July and August, 2009 in which size-resolved flux measurements were made, primarily with an FMPS. To the authors' knowledge, there have been only two direct measurements of size resolved fluxes over forests, one of which was pine (Gronholm et al., 2007) and the other mixed deciduous (Pryor et al., 2009). The results of this study demonstrate a predominance of upward fluxes at this location, allowing for further exploration of the root cause of this phenomenon. Results are presented and compared to previous studies, including the results of a study in which chemically speciated aerosol fluxes were measured with an Aerodyne Quadrupole Aerosol Mass Spectrometer (Q-AMS) at the Borden Forest Flux Tower in July and August of 2006.

2 Method

2.1 Site description

This study took place at the Borden Forest Research Station (44° 19′ N, 79° 56′ W) in Ontario, Canada. The forest is a mix of hardwood and coniferous trees from regrowth on abandoned farm land, with an age of approximately 100 years. The average canopy

ACPD
10, 22469–22513, 2010

height is approximately 23 m. The surrounding area, shown in Fig. 1, is generally flat within a radius of about 4 km. The available forest fetch is about 4.3 km to the south, and 3 km to the SSW. Outside of this range is predominantly grass and cropland, with the town of Angus, Ontario less than 4 km to the ENE and the Canadian Forces Base Borden 5 km to the SE.

2.2 Instrumentation

Instruments were mounted on a 44-m tower. The tower supports an array of instruments for routine measurements of temperature, wind speed, humidity, and fluxes of energy, water vapour, and CO_2. Details of the measurement setup can be found in Lee et al. (1999), Staebler et al. (2000), and Teklemariam et al. (2009).

An FMPS was mounted above the canopy, at a height of 33 m, and was operational from 13 July to 9 August. The FMPS (TSI Inc., Model 3901) is based on electrical aerosol spectrometer technology (Tammet et al., 2002) and measures particle concentration at a maximum rate of 1 Hz in 32 size bins with a manufacturer specified range of 6 to 560 nm electrical mobility diameter. The FMPS was housed in a temperature-controlled enclosure, to reduce instrument variability due to temperature changes. The temperature within the enclosure was maintained at 20±3 °C throughout the study, resulting in a diurnal variation of the instrument sheath air temperature of <1 °C. The FMPS sampled air through a 4-m, 0.635 mm (0.25 inch) outer diameter, stainless steel tube, with a residence time of approximately 0.8 s. A sonic anemometer (Applied Technologies, Inc., ATI) for EC measurements was mounted near the sample inlet. A second FMPS sampled below the canopy, at a height of 2 m a.g.l. and was operational from 13 to 25 July.

Both FMPS instruments were size-calibrated prior to the field study with a reference condensational particle counter (TSI Model 3775, CPC) using both polystyrene latex spheres (Duke Scientific) of known size and NH_4NO_3 particles. The size calibration was done with particles in the 30 to 450 nm range with and without size selection using a TSI Scanning Mobility Particle Sizer. A power-law, least-squares fit gives a relation

ACPD
10, 22469–22513, 2010

between the FMPS specified diameter (D_{FMPS}) and the actual diameter of D=0.29 $D_{FMPS}^{1.31}$ (nm) with r^2=0.984. This gives an actual FMPS size range of 3<D<1060 nm. However, since the calibration was performed with 30 to 450 nm diameter particles only, size estimations of the smallest 9 bins (6<D_{FMPS}<20 nm) and the largest 5 bins (294<D_{FMPS}<523 nm) were not used for flux analysis.

3 Data analysis

Conservation of mass for the scalar concentration C gives (e.g., Businger, 1986)

$$\frac{\partial C}{\partial t} + \frac{\partial}{\partial x_i} u_i C + \frac{\partial}{\partial z}(V_g C) = D_M \frac{\partial^2}{\partial x_i^2} C + S \tag{1}$$

where D_M is the molecular diffusion coefficient, V_g is the gravitational settling velocity, and S is a source or sink term. For small particles (<1 µm) it can be assumed that $V_g \approx 0$ and that the molecular diffusion term is small relative to the other terms. Assuming horizontal homogeneity and steady state, Reynolds decomposition and integration in z to the measurement height, z_r, gives

$$\int_0^{z_r} \frac{\partial \overline{C}}{\partial t}\, dz + \overline{w'C'}(z_r) = \int_0^{z_r} \overline{S}\, dz \tag{2}$$

where the overbar and prime denote mean and fluctuating terms. For simplicity, Eq. (2) is rewritten as

$$F_{Stg} + F = S_T \tag{3}$$

The term S_T is the net sum of sources and sinks below z_r per unit area, and F_{Stg} is the storage flux, so called because a positive concentration change rate below the measurement height is equivalent to a "storage" or build-up of particles in the control volume. Conversely, a negative F_{Stg} is equivalent to a dilution or flushing of particles from

ACPD
10, 22469–22513, 2010

the control volume. Since $F_{Stg} \approx z_r(\overline{C}(t+\Delta t)-\overline{C}(t))/\Delta t$, the storage flux will become negligible if the averaging period, Δt, is large (many days to weeks). From Eq. (3), this gives $\langle F \rangle = \langle S_T \rangle$, where $\langle\,\rangle$ denotes a long-term average. Hence, the average flux will be equal to the average particle creation or removal rate per unit area.

An exchange velocity is defined as $V_e = F/\overline{C} = -V_d$, where V_d is a deposition velocity (with the negative sign added since flux is positive upwards and deposition is positive in a downward direction). For the following analysis, concentrations and fluxes were calculated in 30-min intervals. The concentration data were also filtered for low frequencies by linear de-trending of each 30-min interval.

3.1 Corrections and filtering

In total, n=736 intervals were measured. Only data with wind direction in the range 90 to 255° (Teklemariam et al., 2009) were used since other wind directions represent insufficient homogeneous fetch for flux measurements, as is illustrated in Fig. 1. EC measurements with friction velocity, $u_* < 0.2\,\mathrm{m\,s^{-1}}$ were also removed as they are considered unreliable due to low turbulent mixing (Teklemariam et al., 2009). After filtering for wind direction and friction velocity, the data comprise n=233 intervals (a removal of 68%).

Each 30-min average wind velocity was used to rotate the sonic measurements following Wilczak et al. (2001), with one rotation around the z-axis to give $\overline{v}=0$, and a second rotation around the y-axis to give $\overline{w}=0$. Fluxes were corrected for variation in density due to the flux of water vapour following Webb et al. (1980). This correction was never more than 1%. No correction was made for variation in density due to heat flux, as fluctuations of heat are assumed to be dissipated in the 4-m inlet tube (Rannik et al., 1997).

Fluxes were also corrected for the attenuation of the signal above 1 Hz due to the response time of the instrument, following Horst (1997). This frequency response correction is based on stability z/L, where z is the measurement height and L is the

ACPD
10, 22469–22513, 2010

Monin-Obukhov length. This correction results in an average increase ($\langle F/F_0 \rangle$) of 9.8%, and a total increase ($\langle F \rangle / \langle F_0 \rangle$) of 6.2%, where F and F_0 are the corrected and uncorrected fluxes, resepectively. Detailed summaries of these corrections techniques can be found in Buzorius et al. (2000) and Pryor et al. (2007, 2008c).

Since the absorption or loss of water may change particle size, correlation between relative humidity (RH) and w can result in modified particle number fluxes for size-resolved measurements, when particles move into neighbouring bins due to hygroscopic growth. Two approaches to correcting this problem, which differ in their choice of particle growth formula, are outlined in Kowalski (2001) and Vong et al. (2004). We use here the model of Vong et al., which assumes a particle growth with humidity of

$$\frac{D(\mathrm{RH})}{D_0} = (1 - \mathrm{RH})^{-\gamma}. \quad (4)$$

The hygroscopic growth parameter is assumed to be γ=0.214, which Sweitlicki et al. (2000) suggest for "aged European air". Sensitivity to this parameter is discussed in Sect. 5.8.

As shown in Vong et al. (2004), the deposition velocity correction is

$$\Delta V_\mathrm{d} = \frac{-\beta\gamma\overline{w'q'}}{(q_\mathrm{sat} - q)}, \quad (5)$$

where q is the specific humidity ratio (which gives RH=q/q_sat) and β is the power-law exponent for the particle number size distribution. For D>300 nm, the change in concentration with particle size can be approximated by

$$dC(D)/dD \propto D^{-(\beta+1)}. \quad (6)$$

For D<300 nm, Eq. (6) can be applied to the particle number size distribution for small ΔD and β can be determined using Eq. (6) and the particle number concentrations (C) of two adjacent bins. As with the Webb correction, it is assumed that temperature fluctuations are dampened in the inlet. The fluxes are then corrected as

$$F = F_0 + \Delta V_\mathrm{d}\overline{C}. \quad (7)$$

ACPD
10, 22469–22513, 2010

This correction results in an average number flux increase ($\langle F/F_0 \rangle$) over all size ranges of 26%, and a total decrease ($\langle F \rangle / \langle F_0 \rangle$) of 5.8%.

4 Results

4.1 Measurements

The concentrations measured by the FMPS for the entire period (after filtering) are shown in Fig. 2. The peak number concentration is near 62 nm. The solid line shows the typical FMPS noise with filtered inlet air, as specified by the manufacturer. Hence, a significant number of measurements with D<20 nm and D>410 nm are below the noise level of the instrument. These sizes were not used for flux analysis. As discussed in Sect. 2.2, bins below 29 nm and above 410 nm were not calibrated for size and the sizes shown in Fig. 2 are based on extrapolation of the least-squares fit.

The diurnal variation of the concentration, flux, and exchange velocity of the 62 nm particles are shown in Fig. 3d–f. The number of 30-min samples for each hour after filtering for wind direction and friction velocity are shown (Fig. 3a). To demonstrate the full range of the diurnal cycle, the variation of u_* and the stability, z_r/L are shown without filtering for friction velocity (Fig. 3b,c).

During stable conditions (z_r/L>0), throughout the night, turbulent fluxes and deposition velocities are generally small. During unstable (z_r/L<0) and neutral conditions ($z_r/L \approx 0$), throughout the day, the fluxes are predominantly upward. Figure 3g shows the total exchange velocity for the range 20<D<410 nm. The similar range of V_e for 62 nm and V_e for 20<D<410 nm demonstrates that the 62 nm bin is a good representation of the total measurable size range.

The size resolved number concentration fluxes and exchange velocities for D>16 nm are shown in Fig. 4. Fluxes for 20<D<410 nm are generally upward (positive medians). The fraction of upward fluxes is 60% for all sizes (i.e., 60% of the fluxes were above zero). The exchange velocity is similarly distributed for 24<D<280 nm, with the

ACPD
10, 22469–22513, 2010

majority of the measurements between −0.5 and 2.0 mm s^{-1}, and median values near 0.5 mm s^{-1}.

4.2 Uncertainty

Finite sample lengths introduce an uncertainty into the measurements. The uncertainty, ε, depends on the choice of integration period, the variability of the flux in time, and the degree to which the flux measurement time series correlates with itself when shifted in time. The uncertainty was quantified by Lumley and Panofsky (1964) as

$$\varepsilon^2 = \frac{2\xi}{T}\left[\overline{\left(w'C_i'\right)^2} - \overline{w'C_i'}^2\right] \tag{8}$$

where T=1800 s is the averaging time period, and ξ is the time scale. Rannik et al. (2009) demonstrate that this uncertainty is equivalent to the standard error. Hence, we are 68% confident that that the true value is within the range $F \pm \varepsilon$ and 95% confident that the true value is within the range $F \pm 2\varepsilon$.

The time scale is calculated as

$$\xi = \frac{1}{\sigma_{wC}^2}\int_0^\infty R_{wC}(\tau)d\tau, \tag{9}$$

where $R_{wC}(\tau)$ is the auto-covariance, and $\sigma_{wC}^2 = R_{wC}(0)$ is the variance of $w'C_i'$. Since a long term integration is not practical due to variation over diurnal time-scales (non-stationarity), the integral is evaluated to the first zero-crossing $\tau(R_{wC}=0)$, following Rannik et al. (2009). The error is calculated for each 30-min flux from the 62 nm bin. The fluxes are filtered by wind direction and friction velocity, but are not corrected for frequency response or deliquescence, since we are concerned here with the error value relative to the raw measurement. The distribution of the ratio of the flux (F) to the error (ε) is shown in Fig. 5. Approximately half the data are within $|F|<\varepsilon$, suggesting that these data are not statistically different from F=0 (at a 68% confidence level). At the

ACPD
10, 22469–22513, 2010

95% confidence interval, 19.3% of the fluxes are significantly upward ($F>2\varepsilon$) and 3.4% are significantly downward ($F<2\varepsilon$). This demonstrates that the dominance of upward fluxes is statistically significant and not due to random uncertainties.

4.3 Net storage and source fluxes

Following Rannik et al. (2009), we calculate the storage flux as

$$F_{\mathrm{Stg}} = z_r \frac{C^+(t+T) - C^+(t)}{T} \tag{10}$$

where z_r=33 m, T=1800 s, and $C^+(t)$ and $C^+(t+T)$ are the 120-s averages at the start and end of each 30-min period. This assumes a constant concentration with height. This is supported by a comparison of the 2-m and 33-m FMPS measurements, since the average difference between the 2-m and 33-m particle number concentrations in the 62 nm size bin is relatively small (3%). The results show weak sensitivity to the averaging time, with very little difference in the calculated storage fluxes using averaging times of 30 s and 300 s in Eq. (10).

The average values $\langle F\rangle$ and $\langle F_{\mathrm{Stg}}\rangle$ are compared in Fig. 6 (black and blue lines, respectively). For a very long, periodic time series the average $\langle F_{\mathrm{Stg}}\rangle$ should be negligible. Here, we see a negative storage flux for $D<60$ nm, and a small positive storage flux for $60<D<250$ nm. When unfiltered data is used (n=736), the storage flux is much smaller ($|\langle F_{\mathrm{Stg}}\rangle|<0.08\times10^6$ m^{-2} s^{-1} for all sizes). This suggests a bias in the filtered data towards a decreasing concentration of small particles ($D<60$ nm), and an increasing concentration of mid-range particles ($60<D<250$ nm). The average values of the total source ($\langle S_{\mathrm{T}}\rangle=\langle F_{\mathrm{Stg}}\rangle+\langle F\rangle$) are shown in Fig. 6 (red line). The fraction of S_{T} that is upward is 57%, which is a small change from the 60% fraction of F that is upward.

ACPD
10, 22469–22513, 2010

5 Discussion

Upward fluxes occur in this study with significantly greater frequency than in previous studies over forest locations (see Sect. 1). As shown in Sect. 4.2, these upward fluxes are not associated with random, stochastic error, and remain even after filtering and corrections are applied. Pryor et al. (2008a) investigated the effect of wind direction, assuming a point or line source of emissions, and the angle of attack on the sonic anemometer, which has been shown to give erroneous flux measurements. An investigation (not shown here) of fluxes sorted by wind direction and sonic angle of attack (as determined by the second sonic rotation angle) shows no correlation between flux direction and either variable (r^2<0.01). Hence the fluxes appear to indicate a net source of particles at or below the canopy. Below we investigate the mechanics of the particle formation events and the influence of various effects on the upward particle fluxes.

5.1 Particle growth

Figure 7 shows the time series of concentration for each size bin. Strong particle growth events are seen on DOY 196, past 14:00 UTC, and at the start of DOY 214. Weaker events are seen late in DOY 202, early in DOY 206, and late in DOY 207. Also shown in Fig. 7 is the measured SO_2 mixing ratio. Spikes in the SO_2 mixing ratio coincide with the particle growth episodes listed above. Back trajectories (Meteorological Services Canada) show that air masses on these days were from the nearby cities of Toronto or Detroit, as well as a coal fired power plant (Nanticoke) approximately 170 km south of the tower site. Concentration measurements made by the second FMPS at 2 m are also shown. In these measurements, a daily spike in the concentration near 6 nm at approximately 18:00 UTC is apparent. Both instruments show noise in the lower (4–7 nm) channels, between DOY 205.5 and 208.5 at 33 m and throughout the measurements at 2 m.

The time series of the 8 nm number concentrations measured at 2 m and 33 m are shown in Fig. 8 for DOY 194 to 204. The 8 nm bin (estimated mean diameter) is chosen

ACPD
10, 22469–22513, 2010

to demonstrate the timing of the growth from nucleation mode particles (below the FMPS detection limit) to larger (ca. 62 nm) particles (as shown in Fig. 7). Also shown in Fig. 8 is the incoming solar shortwave (SW) radiation, and the SO_2 mixing ratio. Generally the particle number concentration peaks occur near or soon after the SW peaks. When there is a high SO_2 mixing ratio during the day (e.g. DOY 194, 196, and 202), the peak particle number concentration is generally higher. This can be due to the oxidation of SO_2 to sulphuric acid, which nucleates to form small particles (<2 nm) which could then grow to 60–70 nm.

Due to increased diffusion of smaller particles and increased settling velocity of larger particles, modelled deposition over canopies reaches its minimum between 100 nm and 2 µm. Models summarized in Petroff et al. (2008) estimate the deposition velocity of 20 nm particles over forests at between 1.5 and 40 mm s^{-1}, compared to the estimated V_d for 100 nm particles between 0.25 and 20 mm s^{-1}. Since concentrations are higher during nucleation, the high deposition velocity combined with high concentration would give strong downward fluxes.

In measurements above a pine forest, Mäkelä et al. (1997) determined that the average particle number size distribution has three modes for particles between 2.2 and 600 nm. These modes are D<20 nm, 20<D<110 nm, and 110<D<500 nm, which they describe as nucleation, Aitken, and accumulation modes, respectively. Buzorius et al. (2000) measured fluxes at this location over the same time period and found that the highest downward fluxes occurred when number concentration of particles with D<20 nm was between 5 and 60 times higher than the concentration of particles with 20<D<110 nm. In our study, this ratio ($C(D<20\,\text{nm})/C(20<D<110\,\text{nm})$) is never greater than 4. Mäkelä et al. (1997) demonstrated that the mean particle size takes between 6–12 h to grow from approximately 5–6 nm to 40–70 nm. In our study, the growth is much more rapid, taking between 3 and 7 h for the same amount of growth, based on visual inspection of the time series colour image plots (Fig. 7). This may explain why the fraction of upward fluxes is much higher here than previous studies, since the smaller particles have less time to deposit.

ACPD
10, 22469–22513, 2010

5.2 Effect of precipitation

Precipitation was measured in 15-min intervals at a nearby pond (280 m NE of the tower). In addition to these measurements, leaf wetness was measured at a height of 33 m. Daily precipitation values were also measured at the Egbert station (Climate ID 611E001), which is located 15 km SE of the tower. These three measurements were used to distinguish dry conditions from wet conditions, with wet conditions defined as either non-zero 15-min precipitation, a leaf wetness of more than 10%, or a day with measured precipitation of more than 4 mm. Table 1 compares the fluxes for the 62 nm bin for wet and dry conditions. Fluxes are significantly higher when conditions are dry, for all three precipitation criteria. The largest difference is seen when the leaf wetness criterion is used; however, this may be due to morning condensation, when fluxes are generally lower. A similar difference is also seen using the criterion of daily precipitation, which does not include a diurnal effect since the whole day is classified as either wet or dry. The difference in fluxes between wet and dry conditions is smaller for the 15-min precipitation criterion; however, there are a small number of flux measurements during rain. When the 15-min precipitation measurements are converted to daily totals and the criterion of daily precipitation >4 mm is used, the difference between fluxes on dry days and wet days is more pronounced, with significantly more upward fluxes on dry days. Hence there is an apparent link between the absence of precipitation and upward fluxes. This could be due to increased deposition to wet surfaces, as was found by Erisman and Draaijers (2003).

5.3 Mixing

Ahlm et al. (2009) measured particle fluxes for D>10 nm above the Amazon rain forest. They found that the median fraction of upward fluxes (over a 9 week period) varied from 30 to 55% through the night and morning, then briefly peaked above 70% before midday, after which it remained between 20 and 50% (their Fig. 10). Nilsson et al. (2001) examined particle flux data from a pine forest in Hyytiälä, Finland. They showed results

ACPD
10, 22469–22513, 2010

for a single day (their Fig. 9), during which fluxes were downward, between 0 and $-10^7\,m^{-2}\,s^{-1}$ through the night and into the early morning. A few hours after sunrise, the flux briefly peaked above $5\times10^6\,m^{-2}\,s^{-1}$ (upward), after which it dropped to between $-15\times10^6\,m^{-2}\,s^{-1}$ and $-80\times10^6\,m^{-2}\,s^{-1}$ (downward) for the remainder of the day.

The brief morning peak upward flux was ascribed in both cases to the growth of the mixing layer as it passes the measurement point. This entrains cleaner air from above, resulting in a positive flux measurement. From Eq. (3), this implies a negative storage rate, F_{Stg} caused by the dilution of particles out of the forest, which is balanced by positive flux, F (assuming the source term S_T does not change significantly during this period). Figure 9 shows the fraction of upward fluxes sorted by hour of day during the present study. Here, there is no brief peak between sunrise (10:00 UTC) and midday. The fraction of upward fluxes varies from 20 to 80% throughout the night, then steadily climbs throughout the day after 12:00 UTC, reaching a maximum after 17:00 UTC. This sustained high fraction of upward fluxes suggests that either the positive flux is balanced by a negative storage flux throughout the day (as would occur with a sustained mixing of cleaner air from above), or there is a sustained source of particles generating these upward fluxes.

To investigate the relation between flux and storage flux, the 62 nm bin eddy covariance fluxes are sorted by storage flux and averaged, as shown in Fig. 10. The average values show a pattern which can be modelled as

$$F = \begin{cases} -F_{Stg}, & F_{Stg} < 0 \\ 0, & F_{Stg} > 0 \end{cases}. \quad (11)$$

Despite this pattern, it is noted that nearly 8% of the data are outside of the range ($-3.25\times10^6 < F_{Stg} < 3.25\times10^6\,m^{-2}\,s^{-1}$) shown in the figure, and the correlation between the measured values of F_{62nm} and those determined by Eq. (11) is very low (r^2=0.05), probably owing to the large amount of scatter in the data. However, this simple model generally supports the conclusions of Nilsson et al. (2001) and Pryor et al. (2008a),

ACPD
10, 22469–22513, 2010

who suggested that observed upward fluxes are due to the entrainment of particle-depleted, chemically-aged air from the free troposphere, which would result in a decrease in concentration (negative storage flux). This is also supported by a comparison of the median fluxes during decreasing mean diameter ($F_{62\mathrm{nm}}=0.21\times10^{6}\,\mathrm{m^{-2}\,s^{-1}}$) and increasing mean diameter ($F_{62\mathrm{nm}}=0.33\times10^{6}\,\mathrm{m^{-2}\,s^{-1}}$), since the mixing of chemically-aged air from above should result in an increasing mean diameter, which is associated with a higher upward flux. If it is assumed that Eq. (11) holds over a long-term average, this gives a source term (from Eq. 3) of $S_{\mathrm{T}}=0$ during a negative storage rate, and $S_{\mathrm{T}}=F_{\mathrm{Stg}}$ during a positive storage rate. This implies that, over the long-term, the observed upward fluxes are not an immediate result of particle formation. Instead, particles are created and stored at or below the canopy (with no resulting upward fluxes), until they are later diluted out into the cleaner air above, which results in an observed upward flux. However, this process appears to apply only over a long-term average, since the correlation between measured F_{Stg} and modelled F_{Stg} (from Eq. 11) is very low.

5.4 Daily variation

Although there appears to be a relationship between upward fluxes and negative storage, there is a large amount of scatter in the data and a poor agreement between Eq. (11) and the measurements. This suggests that the model works well on average, but there is a large amount of variation between different days. Below we investigate the evolution of the fluxes and changes in concentration (storage flux) to see how they interact on a day by day basis.

Figure 11 compares the flux (blue line) and concentration (black line) for the 62 nm bin between 15 July and 2 August. Fluxes from times which would normally be filtered for wind direction or low friction velocities are shown (light blue line) for qualitative comparison. Generally, filtered night-time fluxes (shaded regions) were small, and daytime fluxes were positive, as demonstrated in Sect. 4.1. On DOY 196, two strong increases in concentration (positive storage flux) early and late in the day coincided with

ACPD
10, 22469–22513, 2010

downward fluxes. However, between these two increases, fluxes were strongly upward. DOY 202 and 203 were both characterized by a storage of particles through the night, followed by a decrease in concentration (negative storage flux) in the morning, and generally upward fluxes throughout the day. DOY 206 and 212 were similar to DOY 202 and 203, with generally upward fluxes, although the decrease in concentration was delayed until mid-day, and in DOY 212, there was no storage of particles at night (and very few valid flux measurements). Hence, there generally appears to be a correlation between decreasing concentration (negative storage flux) and upward fluxes during the day. DOY 207 and 213 provide an interesting corollary, as fluxes were nearly zero or downward during both days, and the concentrations were continually increasing (DOY 207) or increasing and then nearly constant (DOY 213) throughout the day.

5.5 Decoupling of the canopy space

Measurements of the 62 nm concentration at 2 m are also shown (red line) in Fig. 11. At some points, there was a lag between the 33 m and 2 m time series. This lag was present through the night and in the morning, but disappeared each day during particle growth near peak daylight, as is demonstrated by the coincident peaks near mid-day. It is present during both concentration increase (positive storage flux) and decrease (negative storage flux). Figure 12 shows the diurnal cycle of the lag, with positive lag indicating that the 2-m signal was delayed relative to the 33-m signal. The lag averages approximately 2 h through the night and reaches zero at mid-day. This suggests that particle number concentration changes in mid-canopy were translated to the forest floor (2 m) very slowly at night (timescale 1–2 h), while they were translated to above the canopy (33 m) much faster. As particle laden or particle depleted air is transported above the forest, there may be delay in either mixing particles into or out of the canopy space. This is most likely to be the case during the night and in the early morning, when there is little turbulent mixing (cf. u_* in Fig. 12). During the day, the time scales are roughly equal and particle concentration changes in mid-canopy are translated to the forest floor and to the 33 m level at approximately the same rate. This would explain

ACPD
10, 22469–22513, 2010

why growing particles were stored in the canopy throughout the night without mixing out; whereas during the day, turbulent mixing time scales are much shorter and no lag between time series is seen.

To summarize Sects. 5.1 through 5.5, the results suggest a growth of particles, which typically begins around mid-day. As these particles continued to grow in size and increase in number through the night, they tended to remain below the canopy due to the decreased mixing and longer timescales at night relative to the day. During this increasing number concentration (positive storage flux), fluxes were generally small (Fig. 10). During the day, when mixing increases and timescales are much smaller (Fig. 12), the negative storage flux (decreasing concentration) balances the upward flux (Fig. 10). This results in the diurnal cycles of flux and flux direction which are shown in Figs. 3e and 9, respectively.

5.6 Speciated results

Although no chemically speciated particle flux measurements were made in the 2009 study, we are able to compare our results to those of a previous study which took place at the same location between 19 July and 2 August, 2006. In this previous study, a Quadrupole Aerosol Mass Spectrometer (Q-AMS) was mounted on the same tower at a height of 29 m. The Q-AMS, described in detail in Jimenez et al. (2003), measures the non-refractory components of aerosols of 40 to 700 nm vacuum aerodynamic diameter (D_{va}).

The instrument was alternated between mass spectrum (MS) and jump mass spectrum (JMS) modes every 30 min. In the MS mode, the mass to charge (m/z) ratios of 1 to 300 were scanned every 300 ms and average spectra were output every 15 min. In the JMS mode (Crosier et al., 2007; Nemitz et al., 2008), 10 specific m/z values were recorded at a frequency of 10 Hz, which was post-processed to 1 Hz to reduce measurement noise. Here we concern ourselves with m/z=30 and 46 (particle NO_3^-), m/z=48 and 64 (particle SO_4^{2-}), and m/z=43 (organics). The Q-AMS sampled air

ACPD
10, 22469–22513, 2010

through a 4-m, 0.635 mm (0.25 inch) outer diameter, stainless steel tube, with a residence time less than 0.4 s. A sonic anemometer (ATI) was mounted near the sample inlet, and EC was used to determine mass fluxes, F_m. Details of how EC measurements are made using a Q-AMS can be found in Nemitz et al. (2008). In addition to the standard micrometeorological instrumentation (cf. Lee et al., 1999), a fast-response NH_3/NO_y detector (CLD 88 CYpr, Eco-Physics AG, Switzerland) was used to measure ammonia concentration at 32 m and a Scanning Mobility Particle Sizer (SMPS) measured particle size distributions at 33 m.

Due to technical issues with the Q-AMS, after applying the corrections and filtering outlined in Sect. 3.1, there were only 92 30-min data intervals from the Q-AMS, spread over 12 days. The results showed the aerosol mass to be approximately 52% organics, 34% sulphate, 11% ammonium, and 3% nitrate by mass. Mass flux measurements of SO_4^{2-} demonstrate no directional tendency, with 18% of the data having $F_m < -\varepsilon$ (from Eq. 8), and 18% having $F_m > \varepsilon$. Flux measurements of NO_3^- show a strong downward tendency, with 61% of fluxes with $F_m < -\varepsilon$ and 7% of fluxes with $F_m > \varepsilon$. The average flux and exchange velocities are compared in Table 2 along with other mass fluxes which are discussed in Sect. 5.8 below. The difference between sulphate and nitrate fluxes are comparable to measurements by Thomas (2007) made over an oak forest in Hampshire, UK, where average fluxes of 0.5 and $-5.4\,\mathrm{ng\,m^{-2}\,s^{-1}}$ and exchange velocities of 0.6 and $-17.2\,\mathrm{mm\,s^{-1}}$ were found for SO_4^{2-} and NO_3^-, respectively.

5.7 Ammonium-nitrate evaporation

The NO_3^- deposition velocity follows a diurnal cycle with relatively low values through the night, a peak value between 5 and $20\,\mathrm{mm\,s^{-1}}$ near 12:00 UTC, and decreasing values through the day. A sample day (20 July 2006) is shown in Fig. 13a–f. Wyers and Duyzer (1997) suggested that the downward flux of NO_3^- is due to evaporation of NH_4NO_3 when temperatures increase near the canopy relative to the air aloft. The inset in Fig. 13f shows the temperature in the canopy (<23 m) increasing nearly 1.5 °C

ACPD
10, 22469–22513, 2010

between 10:00 and 10:30 UTC (lightest blue line), while the temperature above the canopy decreased approximately 1 °C (black line), which would give a relative increase in NH_4NO_3 evaporation at the canopy. However, nitrate concentrations continued to decrease (Fig. 13a) between 11:00 and 13:00 UTC, while temperatures were approximately equal at all heights. This implies that some other mechanism may be responsible for the downward NO_3^- fluxes. Further, there is a higher increase in molar NH_3 concentration (96 nmol m^{-3}) than can be accounted for by the decrease in the NO_3^- molar concentration (51 nmol m^{-3}).

To further investigate possible effects of NH_4NO_3 evaporation, the changes in ammonia gas concentration for each hour are compared to the simultaneous NO_3^- flux measurements in Fig. 14 for the two weeks of data. The concentration change is integrated to the measurement height, z_r=29 m. Generally, the high downward NO_3^- fluxes occurred when the NH_3 concentration was increasing. The average NO_3^- flux for $dC_{NH_3}/dt>0$ is more than 3 times larger than the average NO_3^- flux for $dC_{NH_3}/dt<0$, with flux values −69 vs. −21 pmol m^{-2} s^{-1}. This is consistent with NH_4NO_3 evaporation at the canopy, where a decrease in NH_4NO_3 near the canopy (which would cause a NO_3^- gradient) would correlate with an increase in NH_3 concentration. If we assume that the entire NO_3^- flux is due to evaporation below z_r and that NH_3 is well mixed below z_r, then

$$F_{NO_3} = \begin{cases} 0, & dC_{NH_3}/dt < 0 \\ -z_r dC_{NH_3}/dt, & dC_{NH_3}/dt > 0 \end{cases}. \quad (12)$$

In Eq. (12), it is assumed that decreases in NH_3 concentration are due to dilution of the NH_3 into cleaner air. This could be confirmed with NH_3 flux measurements; however, we were not able to make these measurements in this study. Further, it is noted that the opposite night-time effect of NH_4NO_3 condensation is not expected to generate strong upward NO_3^- fluxes, as cooling of the canopy is much more gradual (see Fig. 13f). The cooling also takes place during the night when u_* is low and flux measurements are less reliable. The correlation coefficient of measured F_{NO_3} and F_{NO_3} modelled from Eq. (12)

ACPD
10, 22469–22513, 2010

is r^2=0.26. However, there are many other processes involved, and the stoichiometric imbalance in the example of Fig. 13a suggests that the simultaneous increase of NH_3 and downward fluxes may be due to unrelated phenomena, such as deposition of NO_3^- to the canopy and stomatal emission of NH_3.

5.8 Inter-study comparison

In order to compare the 2006 Q-AMS particle compositional flux study with the 2009 FMPS particle number flux study, an estimated total mass flux is calculated from the FMPS measurements. Assuming densities of 1800 kg m^{-3} for sulphate, 1700 kg m^{-3} for nitrate, a weighted average of the sulphate and nitrate densities for ammonium, and 1200 kg m^{-3} for organics, the average density of the aerosols sampled by the Q-AMS is approximately 1500 kg m^{-3}. The size range of the Q-AMS is $40<D_{va}<700$ nm vacuum aerodynamic diameter. Assuming spherical particles, this gives an equivalent size range for the FMPS of $27<D<470$ nm electrical mobility diameter. The total mass flux measured by the FMPS for this size range is listed in Table 2, and the distribution is shown in Fig. 15.

To estimate ammonium fluxes, we assume as an approximation that NH_4NO_3 and $(NH_4)_2SO_4$ are the primary nitrates and sulphates, respectively. Hence, the concentration of NH_4^+ can be determined by molar balance from the JMS mode measurements of NO_3^- and SO_4^{2-}. This assumption can be checked using the concentrations of NO_3^-, SO_4^{2-}, and NH_4^+ measured in the MS mode. The correlation of the concentration (C_{NH_4}) to that determined using the NO_3^- and SO_4^{2-} concentrations is r^2=0.97. This assumption is then used to calculate ammonium fluxes from the nitrate and sulphate fluxes. The mean and standard deviation of the ammonium fluxes are listed in Table 2 and the distribution is shown in Fig. 15.

A comparison of the m/z=43 signal (measured in the JMS mode) and the total organic aerosol mass (measured in the MS mode) gave a coefficient of correlation of r^2=0.86 for the duration of the study. This relation was then used to calculate the total

ACPD
10, 22469–22513, 2010

organic mass fluxes, assuming a constant ratio between the m/z=43 signal and the total organic aerosol mass. The calculated organic mass fluxes (Fig. 15) tend to be larger than the NO_3^-, SO_4^{2-}, and NH_4^+ fluxes, and the standard deviation of the distribution is comparable to that of the FMPS mass flux distribution (Table 2). However, the organic mass fluxes show no significant directional tendency, with 6% of the fluxes significantly upward ($F>2\varepsilon$) and 5% of the fluxes significantly downward ($F<2\varepsilon$). Further, the mean flux (Table 2) is not different from zero at the 95% confidence level.

The two measured (NO_3^- and SO_4^{2-}) and two approximated (NH_4^+ and organic) mass fluxes are combined to determine a total mass flux. The mean, standard deviation, and confidence interval for the total mass flux are listed in Table 2, and the distribution is shown in Fig. 15. The mean flux is significantly different from zero at a 95% confidence level, although the exchange velocity is not. This difference between the mean flux and exchange velocity suggests that the stronger downward fluxes are associated with higher concentrations than the upward fluxes. The most striking difference between the total mass flux distributions from the two studies is the skewness (−0.4 for the Q-AMS total and 1.2 for the FMPS total) with many strong upward fluxes ($F_m>30\,\mathrm{ng\,m^{-2}\,s^{-1}}$) in the 2009 study, and many strong downward fluxes ($F_m<-30\,\mathrm{ng\,m^{-2}\,s^{-1}}$) in the 2006 study. It is unclear what could cause this difference between the studies. One possibility is an undetermined organic flux, since the correlation between m/z=43 and the total organic aerosol mass is only r^2=0.86. There may be one or multiple organics that have relatively low concentrations, but contribute a strong relative component to the total mass flux. The unresolved particles could result in large positive fluxes.

We investigated whether the difference between studies might be due to the water content of the particles, since water content is not included in the calculated Q-AMS total mass flux. A significant upward H_2O vapour flux, which occurs each day, results in a higher water content in upward moving particles, leading to a "false" upward flux of particle mass (cf. Vong et al., 2004). Although the FMPS sizing measurements include the increased size due to particle water content, the "false" upward flux due to an upward H_2O vapour flux is removed by the deliquescence correction described

ACPD
10, 22469–22513, 2010

in Sect. 3.1. To determine the sensitivity of the particle mass flux distribution to the hygroscopic growth parameter, γ, the fluxes we recalculated using γ=0 (no correction) and γ=0.255 (an upper limit based on the results of Swietlicki et al., 2000). Both resulting mass flux distributions are similar (57% of mass fluxes are upward in both cases), suggesting that upward H_2O vapour flux has little effect of the total mass flux.

It is possible that differing conditions between the studies could result in net deposition in the 2006 study and a net source of particles in the 2009 study. Both studies had SO_2 concentrations above ambient levels for a similar fraction of time (between 12 and 15%, depending on the ambient threshold value). Precipitation levels were also similar, with slightly more than 40 mm in the approximately 2 week duration of both studies. SMPS measurements in the 2006 study also demonstrate similar particle size growth episodes and similar size distributions when compared to the 2009 FMPS measurements. Air temperatures during the 2006 study were generally higher, with daily maxima ranging from 24 to 37 °C, compared to daily maxima ranging from 20 to 27 °C during the 2009 study. The average daily mean temperature was 23 °C during the 2006 study and 18 °C during the 2009 study. However, it is unclear how the temperature would affect particle deposition or particle nucleation.

6 Conclusions

Flux measurements in the summer of 2009 demonstrate a significant amount of upward fluxes over this mixed forest location. The fraction of upward fluxes seen in this study (60%) is higher than any previously reported fractions over forests, which range near 20% (Gronholm et al., 2007) to over 40% (Pryor et al., 2008c). The forest is a source of particles at this location with an average source rate less than 0.5×10^6 particles $m^{-2}\,s^{-1}$. This source rate is highest for sizes near 75 nm.

There is particle growth each day, which takes place at or soon after the peak solar radiation. During particle growth, the concentrations tend to be much higher when SO_2 is present, suggesting that SO_2 may be oxidized to H_2SO_4, nucleate, and grow to larger

ACPD
10, 22469–22513, 2010

particles. The particles grow faster at this location compared to measurements above a pine forest (Mäkelä et al., 1997). This may explain the higher fraction of upward fluxes seen here, as the smaller particles have less time to deposit to the canopy. Upward fluxes are also associated with days without precipitation; during precipitation, reduced upward fluxes may be due to increased deposition to wet surfaces, or less particle creation during wet days.

Previous suggestions for upward fluxes included sources of particles within or close to the canopy top (Buzorius et al., 1998), or the entrainment of clean, particle depleted air from above (Pryor et al. 2008a). What is seen in this study combines both effects. Generally, there is an association between decreasing concentration (negative storage flux) and upward fluxes, while average fluxes are very small during increasing concentration (positive storage flux). Due to the decoupling of the above and below canopy spaces, particles are created and stored within the canopy, and then diluted through mixing with the chemically aged, cleaner air above. On average, this creates a positive flux during net depletion of particles from the forest.

Chemically speciated flux measurements from a 2006 study at the same location suggest that there is no significant gradient of sulphate or organic aerosol concentrations and there is a significant positive gradient (increasing with height) of nitrate and ammonium concentration above the canopy, possibly enhanced by the evaporation of ammonium-nitrate at the canopy at sunrise. Estimating the NH_4^+ and organic mass fluxes gives a total mass flux distribution which is skewed toward strong downward fluxes, in contrast to the strong upward fluxes seen in the 2009 study. Conditions (e.g. SO_2, particle growth, precipitation) are similar in both studies, with the exception of temperature, which was 5 °C higher (average daily mean) during the 2006 study. The difference in mass flux distributions could be due to unresolved organic particles, which could be responsible for strong upward fluxes. If this is the case, further research is required to identify this source of aerosols and to isolate the mechanisms for their formation.

ACPD
10, 22469–22513, 2010

Acknowledgements. This work was supported by the Natural Science and Engineering Research Council of Canada and was funded by the Science and Technology Branch, Environment Canada. The authors thank Alexandre Petroff for insight and suggestions, Greg Evans for the use of one FMPS, and the Canadian Forces Base Borden for hosting the Flux Tower site.

References

Ahlm, L., Nilsson, E. D., Krejci, R., Mårtensson, E. M., Vogt, M., and Artaxo, P.: Aerosol number fluxes over the Amazon rain forest during the wet season, Atmos. Chem. Phys., 9, 9381–9400, doi:10.5194/acp-9-9381-2009, 2009.

Bleyl, M. R.: Experimentelle Bestimmung der Depositionsgeschwindigkeit luftgetragener Partikel mit Hilfe der Eddy–Kovarianzmethode über einem Fichtenaltbestand im Solling, Ph.D. thesis (in German), University of Göttingen, Göttingen, Germany, 2001.

Businger, J. A.: Evaluation of the accuracy with which dry deposition can be measured with current micrometeorological techniques, J. Clim. Appl. Meteorol., 25, 1100–1124, 1986.

Buzorius, G., Rannik, Ü., Mäkelä, J. M., Vesala, T., and Kulmala, M.: Vertical aerosol particle fluxes measured by eddy covariance technique using condensational particle counter, J. Aerosol. Sci., 29(1/2), 157–171, 1998.

Buzorius, G., Rannik, Ü., Mäkelä, J. M., Keronen, P., Vesala, T., and Kulmala, M.: Vertical aerosol fluxes measured by the eddy covariance method and deposition of nucleation mode particles above a Scots pine forest in Southern Finland, J. Geophys. Res., 105(D15), 19905–19916, 2000.

Buzorius, G., Rannik, Ü., Nilsson, D., and Kulmala, M.: Vertical fluxes and micrometeorology during aerosol particle formation events, Tellus, 53B, 394–495, 2001.

Crosier, J., Jimenez, J. L., Allan, J. D., Bower, K. N., Williams, P. I., Alfarra, R., Canagaratna, M. R., Jayne, J. T., Worsnop, D. R., and Coe, H.: Technical Note: Description and use of the New Jump Mass Spectrum Mode of Operation for the Aerodyne Quadrupole Aerosol Mass Spectrometer (QAMS), Aerosol Sci. Tech., 41, 865–872, 2007.

Erisman, J. W. and Draaijers, G.: Deposition to forests in Europe: most important factors influencing dry deposition and models used for generalisation, Environ. Pollut., 124(3), 379–388, 2003.

Gaman, A., Rannik, Ü., Aalto, P., Pohja, T., Siivola, E., Kulmala, M., and Vesala, T.: Relaxed

ACPD

10, 22469–22513, 2010

eddy accumulation system for size-resolved aerosol particle flux measurements, J. Atmos. Ocean. Tech., 21, 933–943, 2004.
Grönholm, T., Aalto, P. P., Hiltunen, V., Rannik, Ü., Rinne, J., Laakso, L., Hyvönen, S., Vesala, T., and Kulmala, M.: Measurements of aerosol particle dry deposition velocity using the relaxed eddy accumulation technique, Tellus, 59B, 381–386, 2007.
Held, A. and Klemm, O.: Direct measurement of turbulent particle exchange with a twin CPC eddy covariance system, Atmos. Environ., 40, 92–102, doi:10.1016/j.atmosenv.2005.09.092, 2006.
Horst, T. W.: A simple formula for attenuation of eddy fluxes measured with first-order-response scalar sensors, Bound.-Lay. Metoerol., 82, 219–233, 1997.
Intergovernmental Panel on Climate Change: Climate Change 2007: The Physical Science Basis. Contribution of Working Group I to the Fourth Assessment Report of the Intergovernmental Panel on Climate Change, edited by: Solomon, S., Qin, D., Manning, M., Chen, Z., Marquis, M., Averyt, K. B., Tignor, M., and Millers, H. L., 996 pp., Cambridge Univ. Press, Cambridge, UK, 2007.
Jimenez, J. L., Jayne, J. T., Shi, Q., Kolb, C. E., Worsnop, D. R., Yourshaw, I., Seinfeld, J. H., Flagan, R. C., Zhang, X., Smith, K. A., Morris, J. W., and Davidovits, P.: Ambient aerosol sampling using the Aerodyne Aerosol Mass Spectrometer, J. Geophys. Res., 108(D7), 8425–8438, doi:10.1029/2001JD001213, 2003.
Kowalski, A.: Deliquescence induces eddy covariance and estimable dry deposition errors, Atmos. Environ., 35, 4843–4851, 2001.
Lamaud, E., Brunet, Y., Labatut, A., Lopez, A., Fontan, J., and Druilhet, A.: The Landes experiment: biosphere-atmosphere exchanges of ozone and aerosol particles above a pine forest, J. Geophys. Res., 99, 16511–16521, 1994.
Lee, X. H., Fuentes, J. D., Staebler, R. M., and Neumann, H. H.: Long-term observation of the atmospheric exchange of CO_2 with a temperate deciduous forest in Southern Ontario, Canada, J. Geophys. Res.-Atmos., 104(D13), 15975–15984, 1999.
Lippmann, M.: Environmental Toxicants, Wiley Interscience, New York, 2009.
Lumley, J. L. and Panofsky, H. A.: The Structure of Atmospheric Turbulence. Wiley Interscience, New York, 1964.
Mäkelä, J. M., Aalto, P., Jokinen, V., Pohja, T., Nissinen, A., Palmroth, S., Markkanen, T., Seitsonen, K., Lilavainen, H., and Kulmala, M.: Observations of ultrafine aerosol particle formation and growth in boreal forest, Geophys. Res. Lett., 24(10), 1219–1222, 1997.

ACPD
10, 22469–22513, 2010

Malm, W. C.: Fundamentals of visibility, in: Handbook of Weather, Climate and Water: Atmospheric Chemistry, Hydrology, and Societal Impacts, edited by: Potter, D. T. and Colman, B. R., John Wiley, Hoboken, NJ, 285–329, 2003.

Nemitz, E., Jimenez, J. L., Huffman, A., Ulbrich, I. M., Canagaratna, M. R., Worsnop, D. R., and Guenther, A. B.: An Eddy-covariance system for the measurement of surface/atmosphere exchange fluxes of submicron aerosol chemical species – first application above an urban area, Aerosol Sci. Tech., 42, 636–657, 2008.

Nilsson, E. D., Rannik, Ü., Kulmala, M., Buzorius, G., and O'Dowd, C. D.: Effects of continental boundary layer evolution, convection, Tellus, 53B, 441–461, 2001.

Petroff, A., Mailliat, A., Amielh, M., and Anselmet, F.: Aerosol dry deposition on vegetative canopies. Part I: Review of present knowledge, Atmos. Environ., 42(16), 3625–3653, doi:10.1016/j.atmosenv.2007.09.043, 2008.

Pryor, S. C.: Size resolved particle deposition velocities of sub-100 nm diameter particles over a forest, Atmos. Environ., 40, 6192–6200, 2006.

Pryor, S. C., Larsen, S. E., Sørensen, L. L., Barthelmie, R. J., Grönholm, T., Kulmala, M., Launiainen, S., Rannik, Ü., and Vesala, T.: Particle fluxes over forests: analyses of flux methods and functional dependencies, J. Geophys. Res., 112, D07205, doi:10.1029/2006JD008066, 2007.

Pryor, S. C., Barthelmie, R. J., Sørensen, L. L., Larsen, S. E., Sempreviva, A. M., Grönholm, T., Rannik, Ü., Kulmala, M., and Vesala, T.: Upward fluxes of particles over forests: when, where, why?, Tellus, 60B, 372–380, 2008a.

Pryor, S. C., Gallagher, M., Sievering, H., Larsen, S. E., Barthelmie, R. J., Birsan, F., Nemitz, E., Rinne, J., Kulmala, M., Grönholm, T., Taipale, R., and Vesala, T.: A review of measurement and modelling results of particle atmosphere–surface exchange, Tellus, 60B, 42–75, 2008b.

Pryor, S. C., Larsen, S. E., Sørensen, L. L., and Barthelmie, R. J.: Particle fluxes above forests: observations, methodological considerations and method comparisons, Environ. Pollut., 152, 667–678, doi:10.1016/j.envpol.2007.06.068, 2008c.

Pryor, S. C., Barthelmie, R. J., Spaulding, A. M., Larsen, S. E., and Petroff, A.: Size-resolved fluxes of sub-100-nm particles over forests, J. Geophys. Res., 114, D18212, doi:10.1029/2009JD012248, 2009.

Rannik, Ü., Vesela, T., and Keskinen, R.: On the dampening of temperature fluctuations in a circular tube relevant to eddy covariance measurement technique, J. Geophys. Res., 102(D11), 12789–12794, 1997.

ACPD

10, 22469–22513, 2010

Rannik, Ü., Mammarella, I., Aalto, P., Keronen, P., Vesala, T., and Kulmala, M.: Long-term aerosol particle flux observations. Part I: Uncertainties and time-average statistics, Atmos. Environ., 43(21), 3431–3439, doi:10.1016/j.atmosenv.2009.02.049, 2009.

Spranger, T., Lorenz, U., Gregor, H. D. (eds.): Manual on Methodologies and Criteria for Modelling and Mapping Critical Loads and Levels and Air Pollution Effects, Risks and Trends, Federal Environment Agency, Berlin, 2004.

Staebler, R. M., Fuentes, J. D., Lee, X. H., Puckett, K. J., Neumann, H. H., Deary, M. J., and Arnold, J. A.: Long term flux measurements at the Borden forest, CMOS Bull. SCMO, 28(1), 9–16, 2000.

Swietlicki, E., Zhou, J., Covert, D. S., Hameri, K., Busch, B., and 11 others: Hygroscopic properties of aerosol particles in the Northeastern Atlantic during ACE-2, Tellus, 52B, 201–227, 2000.

Teklemariam, T., Staebler, R. M., and Barr, A. G.: Eight years of carbon dioxide exchange above a mixed forest at Borden, Ontario, Agr. Forest Meteorol., 149, 2040–2053, doi:10.1016/j.agrformet.2009.07.011, 2009.

Tammet, H., Murmee, A., and Tamm, E.: Electrical aerosol spectrometer of Tartu University, Atmos. Res., 62, 315–324, doi:10.1016/S0169-8095(02)00017-0, 2002.

Thomas, R. M.: Measurement of speciated aerosol fluxes, Ph.D. thesis, University of Manchester, Manchester, UK, 2007.

Vong, R. J., Vickers, D., and Covert, D. S.: Eddy correlation measurements of aerosol deposition to grass, Tellus, 56B, 105–117, 2004.

Webb, E., Pearman, G., and Leuning, R.: Correction of flux measurements for density effects due to heat and water vapour transfer, Q. J. Roy. Meteor. Soc., 106, 85–100, 1980.

Wilczak, J. M., Oncley, S. P., and Stage, S. A.: Sonic anemometer tilt correction algorithms, Bound.-Lay. Met., 99, 127–150, 2001.

Wyers, G. P. and Duyzer, J. H.: Micrometeorological measurements of the dry deposition flux of sulphate and nitrate aerosols to coniferous forest, Atmos. Environ., 31(3), 333–343, 1997.

ACPD

10, 22469–22513, 2010

Table 1. Quartiles of 62 nm bin fluxes (10^6 m^{-2} s^{-1}) and number of observations, *n*, for wet and dry conditions as determined by various measurement types.

Measurement	Wet				Dry			
	25th	Median	75th	*n*	25th	Median	75th	*n*
15-min precip (Pond)	−0.18	0.031	0.23	30	−0.11	0.077	0.55	328
Leaf wetness	−0.16	0.021	0.25	120	−0.07	0.111	0.68	238
Daily obs. (Egbert)	−0.20	0.026	0.31	153	−0.05	0.109	0.65	205
Daily obs. (Pond)	−0.18	0.026	0.26	143	−0.06	0.126	0.66	215

ACPD
10, 22469–22513, 2010

Table 2. Average sulphate, nitrate, ammonium, and organic mass fluxes, $\langle F_m \rangle$, and exchange velocities, $\langle V_e \rangle$, with standard deviations, σ, and 95% confidence intervals, *CI*. Organic mass flux is determined from the m/z=43 value. Also shown are the total mass flux and deposition velocity for both the 2006 Q-AMS and the 2009 FMPS measurements in the equivalent Q-AMS size range.

	$\langle F_m \rangle$	σ_F	CI_F	$\langle V_e \rangle$	σ_{V_e}	CI_{V_e}
	ng m^{-2} s^{-1}			mm s^{-1}		
SO_4^{2-}	−1.4	10.7	2.2	−0.3	3.2	0.7
NO_3^-	−4.0	7.0	1.4	−5.1	6.9	1.4
NH_4^+	−1.5	4.2	0.9	−1.3	3.5	0.7
Org.	−3.0	24.2	5.0	−0.2	3.6	0.8
Total	−9.9	30.1	6.2	−0.6	2.7	0.6
FMPS	8.4	27.1	3.6	1.1	2.8	0.4

ACPD
10, 22469–22513, 2010

Fig. 1. Borden and surrounding area. Red dot shows tower location. Arrows show range of wind direction with adequate fetch. Photo reproduced from google.com.

ACPD
10, 22469–22513, 2010

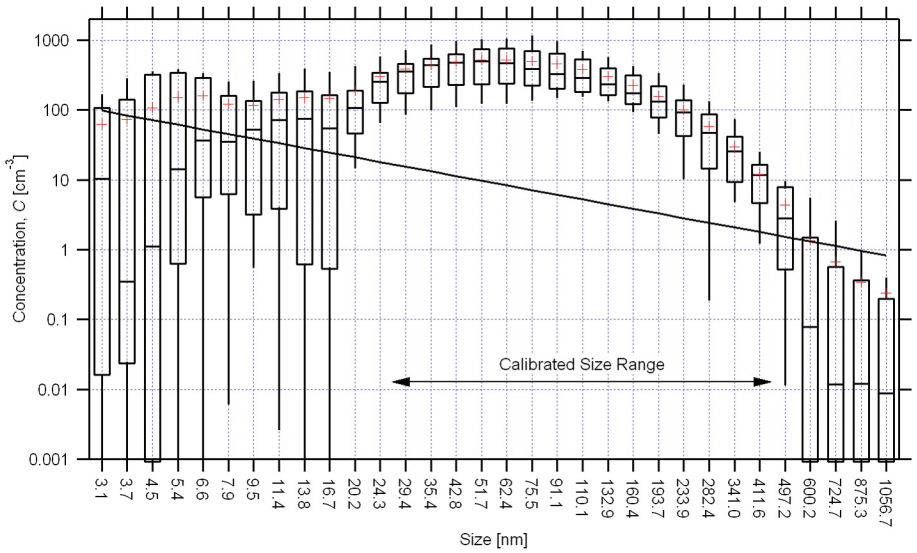

Fig. 2. Percentiles of concentration by size bin. Error lines show 10 and 90%, boxes show 25 and 75%, and centre-line shows medians. Average values shown as (+). Solid line shows the typical FMPS noise with filtered inlet air. Sizes in the calibrated range are shown. Outside this range, sizes are based on extrapolation of the calibrated best fit.

ACPD
10, 22469–22513, 2010

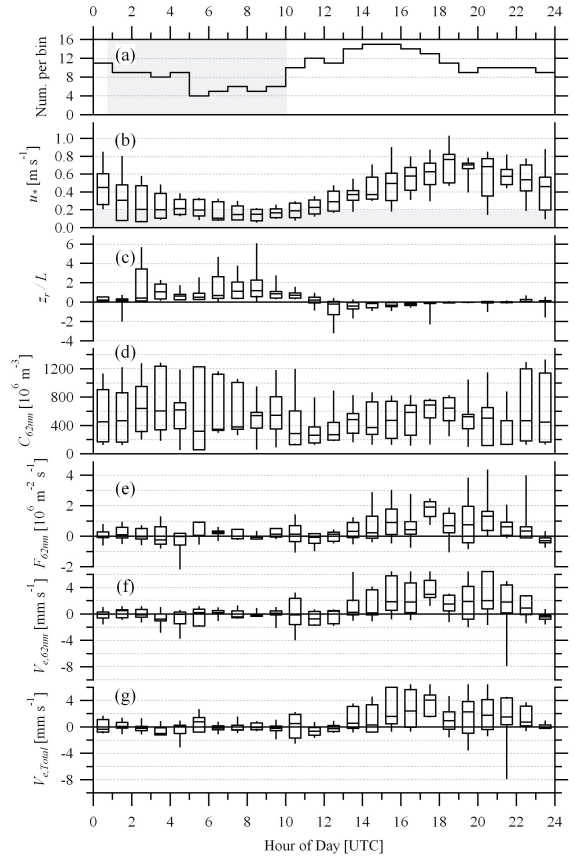

Fig. 3. Percentiles (10, 25, 50, 75, and 90%) of the diurnal variation in friction velocity, u_* **(b)**, stability, z_r/L **(c)**, concentration, $C_{62\text{nm}}$ **(d)**, flux, $F_{62\text{nm}}$ **(e)**, exchange velocity, $V_{\text{e},62\text{nm}}$ **(f)** of the 62 nm bin, and exchange velocity, $V_{\text{e,Total}}$ **(g)** of the total size range ($20<D<410$ nm). Number of 30-min measurements shown (a). Shading indicates night-time (a) and $u_*<0.2\,\text{m s}^{-1}$ (b).

ACPD
10, 22469–22513, 2010

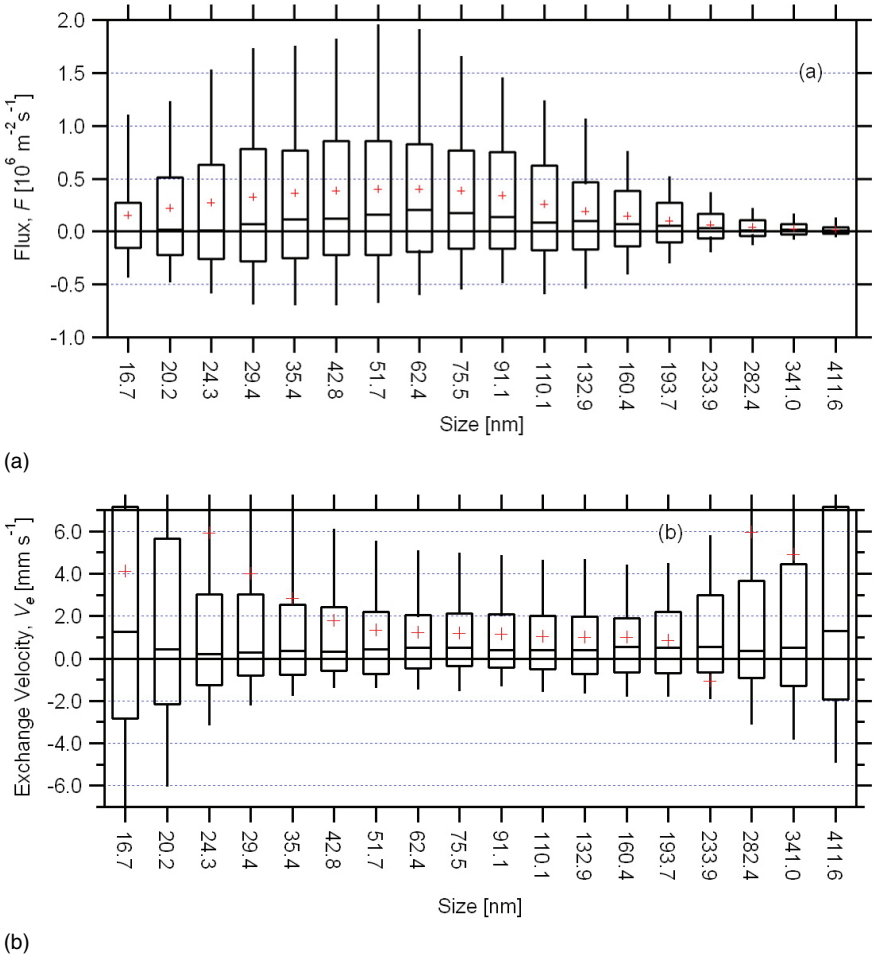

Fig. 4. Percentiles (10, 25, 50, 75, and 90%) and averages (+) of fluxes **(a)** and exchange velocities **(b)** by size bin.

ACPD
10, 22469–22513, 2010

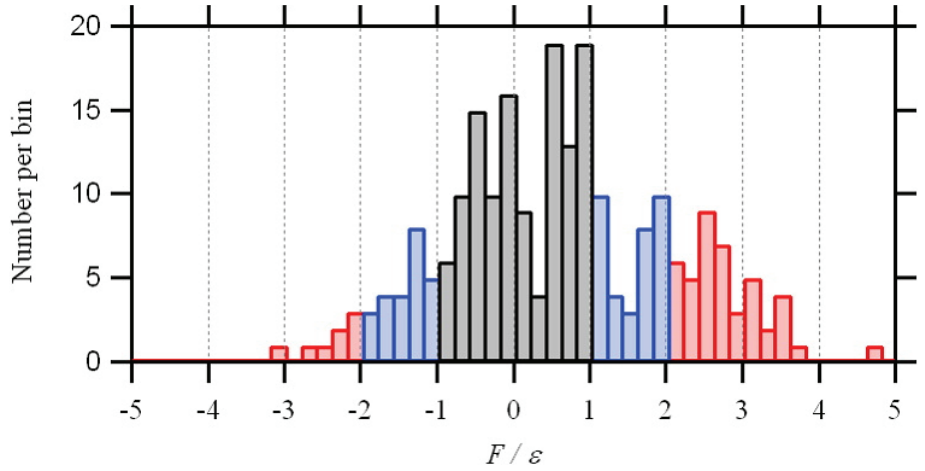

Fig. 5. Distribution of the ratio F/ε for the 62 nm particles. Blue and red bars show measurements which differ from 0 with a 68% confidence and red bars show measurements which differ from 0 with a 95% confidence.

ACPD
10, 22469–22513, 2010

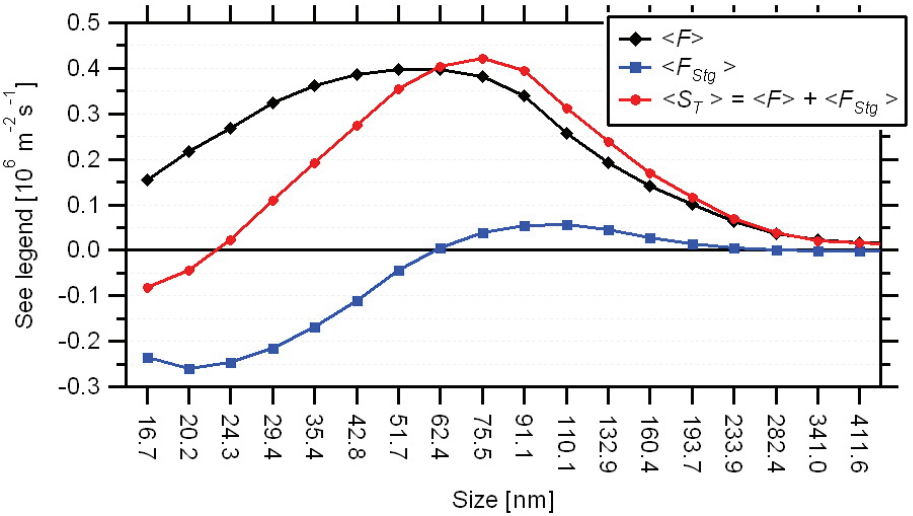

Fig. 6. Average flux, $\langle F \rangle$, storage rate, $\langle F_{Stg} \rangle$, and source rate, $\langle S_T \rangle$, by size bin.

ACPD
10, 22469–22513, 2010

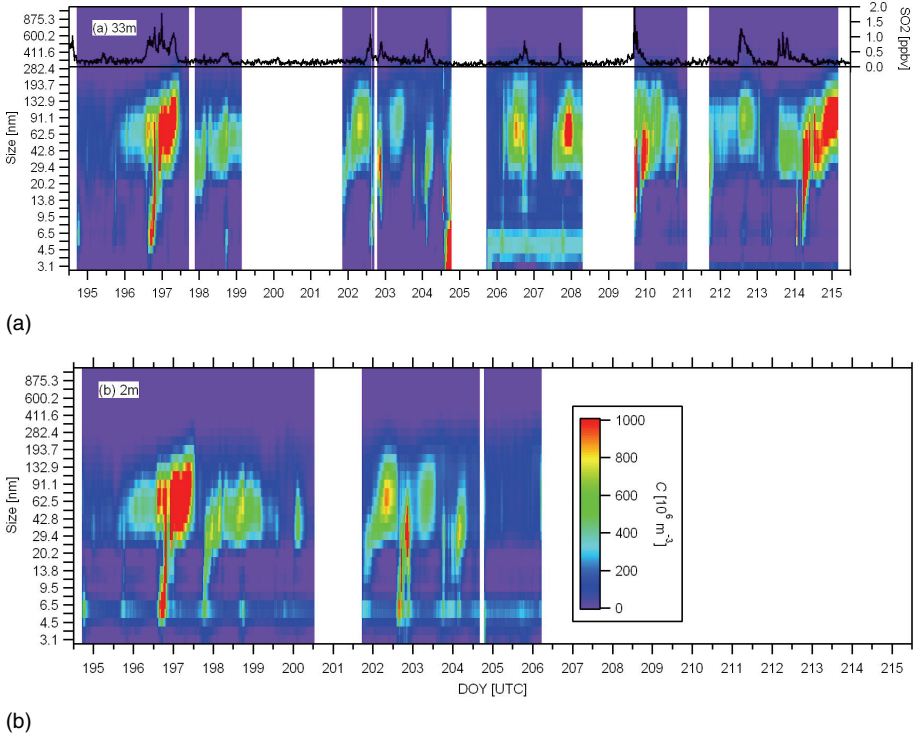

Fig. 7. Time series colour image plots of number concentration by size bin at 33 m **(a)** and 2 m **(b)**. White space is due to instrument error. Time series of SO_2 (black line) at 33 m (a) also shown.

ACPD
10, 22469–22513, 2010

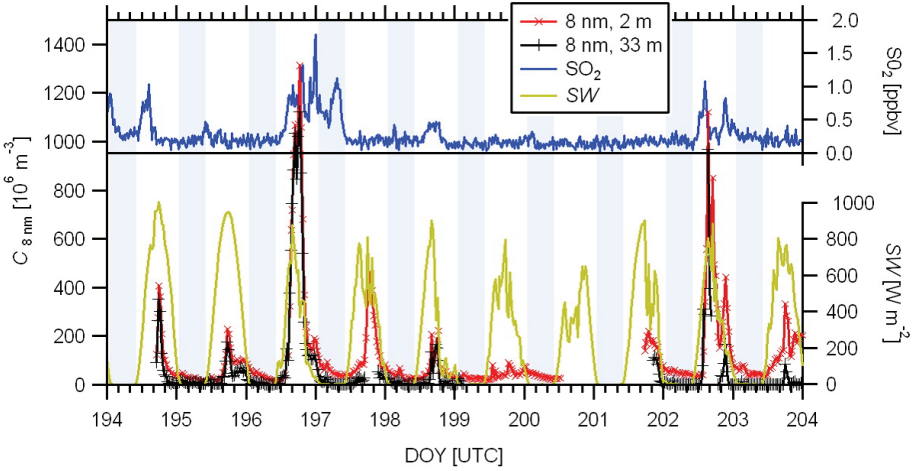

Fig. 8. Time series of 8 nm number concentrations at 2 m and 33 m heights. Time series of SO_2 and downward shortwave radiation (*SW*) also shown. Nights are shaded.

ACPD
10, 22469–22513, 2010

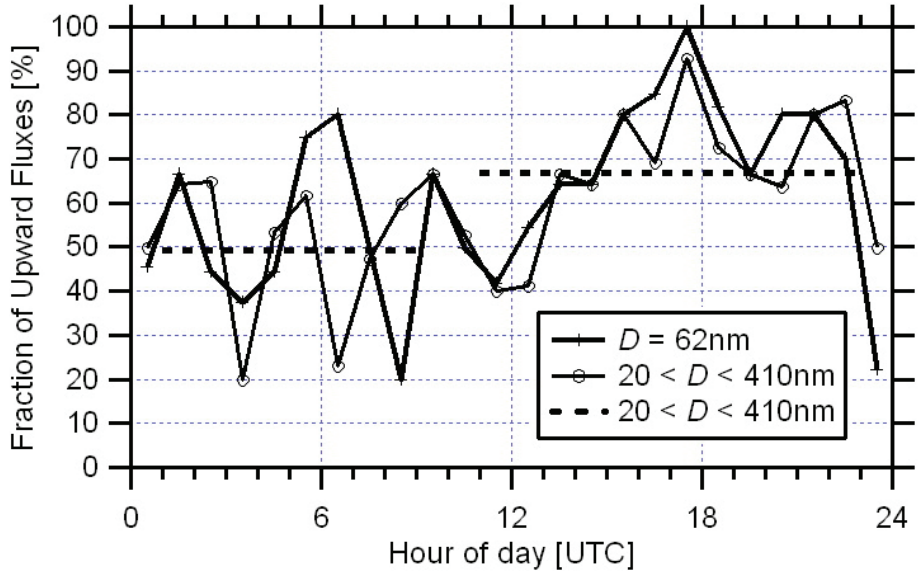

Fig. 9. Fraction of upward fluxes by hour of day. Average values for night (01:00–09:00 UTC) and day (11:00–23:00 UTC) also shown (dashed lines).

ACPD
10, 22469–22513, 2010

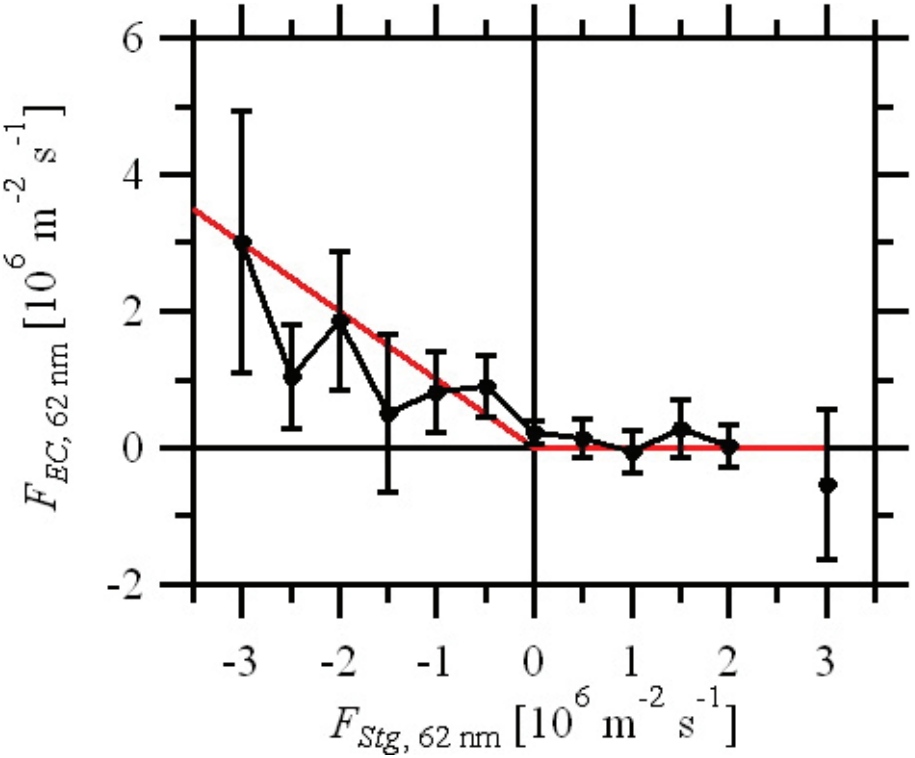

Fig. 10. Average eddy covariance fluxes binned by storage flux for 62 nm particles. Error bars show the 95% confidence interval.

ACPD
10, 22469–22513, 2010

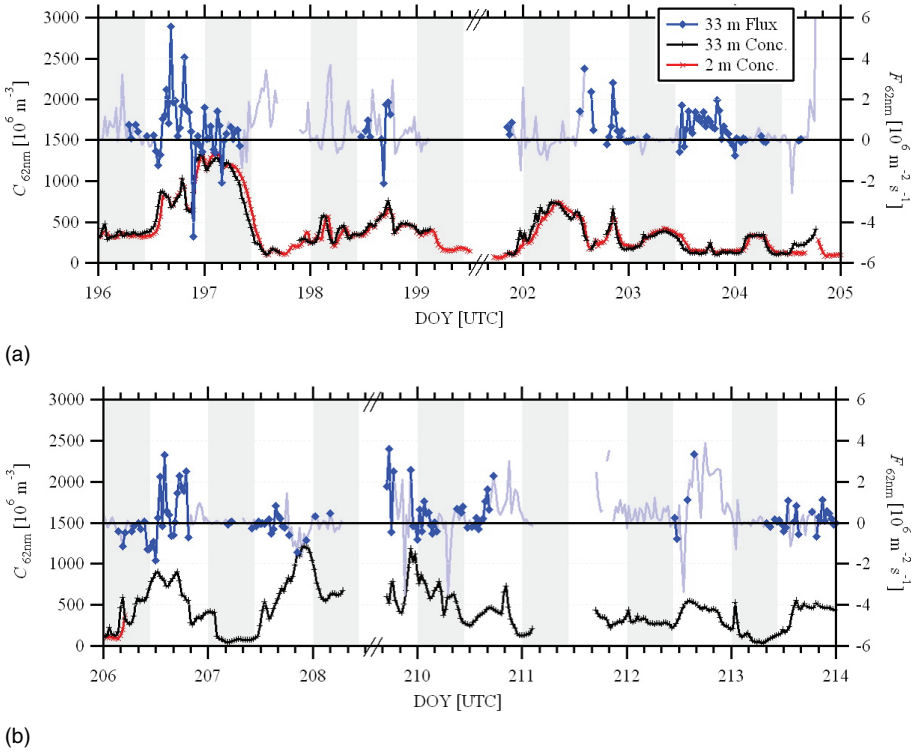

Fig. 11. Concentrations (33 m and 2 m) and fluxes (33 m) for the 62 nm bin. Nights are shaded.

ACPD
10, 22469–22513, 2010

Aerosol flux measurements above a mixed forest at Borden, Ontario

M. Gordon et al.

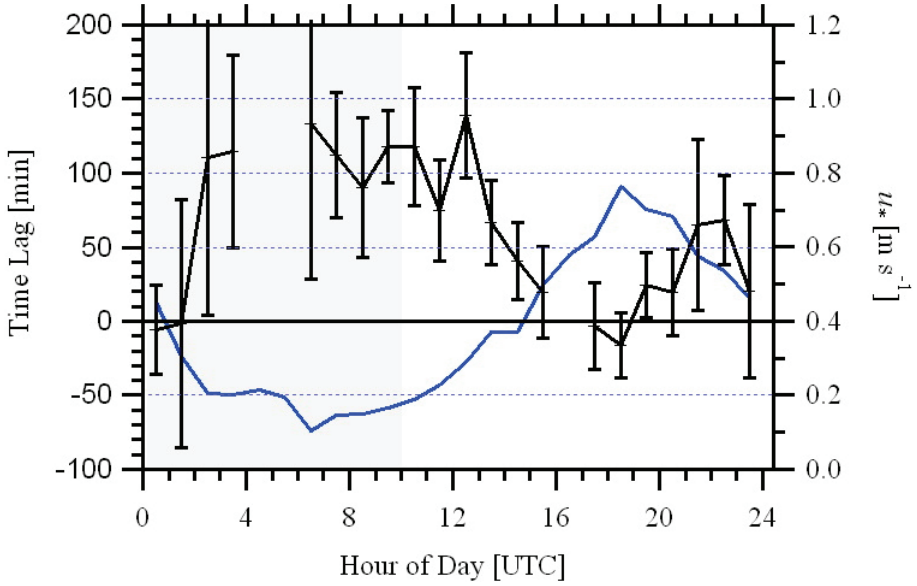

Fig. 12. Average time lag of 2-m concentration signal behind 33-m signal sorted by hour of day. Error bars show 95% confidence interval. Median friction velocity (from 33-m) also shown (blue line). Night is shaded.

ACPD
10, 22469–22513, 2010

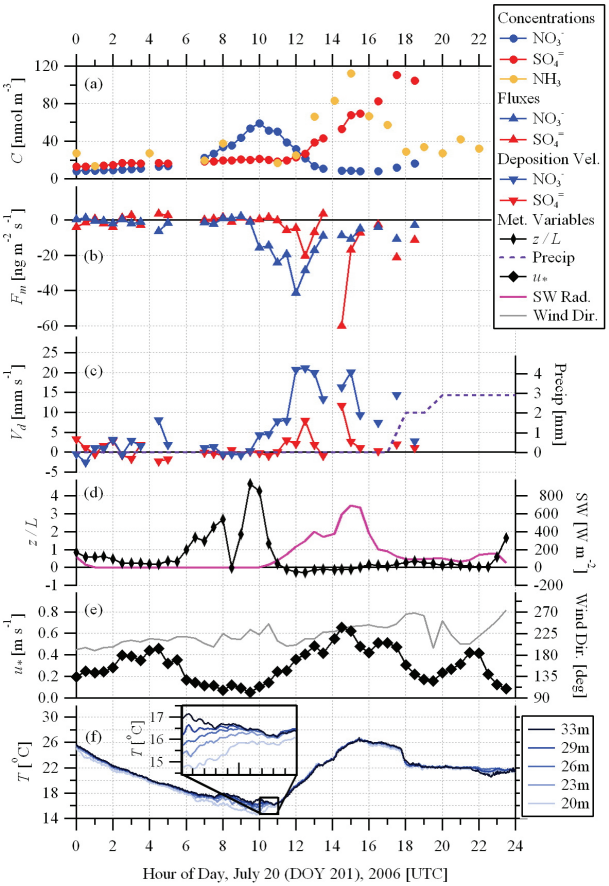

Fig. 13. NO_3^- and SO_4^{2-} concentrations **(a)**, mass fluxes **(b)**, and deposition velocities **(c)**, compared to NH_3 concentration (a) and other meteorological variables (**d** and **e**) on 20 July 2006. Temperatures at various heights are shown **(f)**. Inset in (f) shows temperatures from 10:00 to 11:00 UTC.

ACPD
10, 22469–22513, 2010

Aerosol flux measurements above a mixed forest at Borden, Ontario

M. Gordon et al.

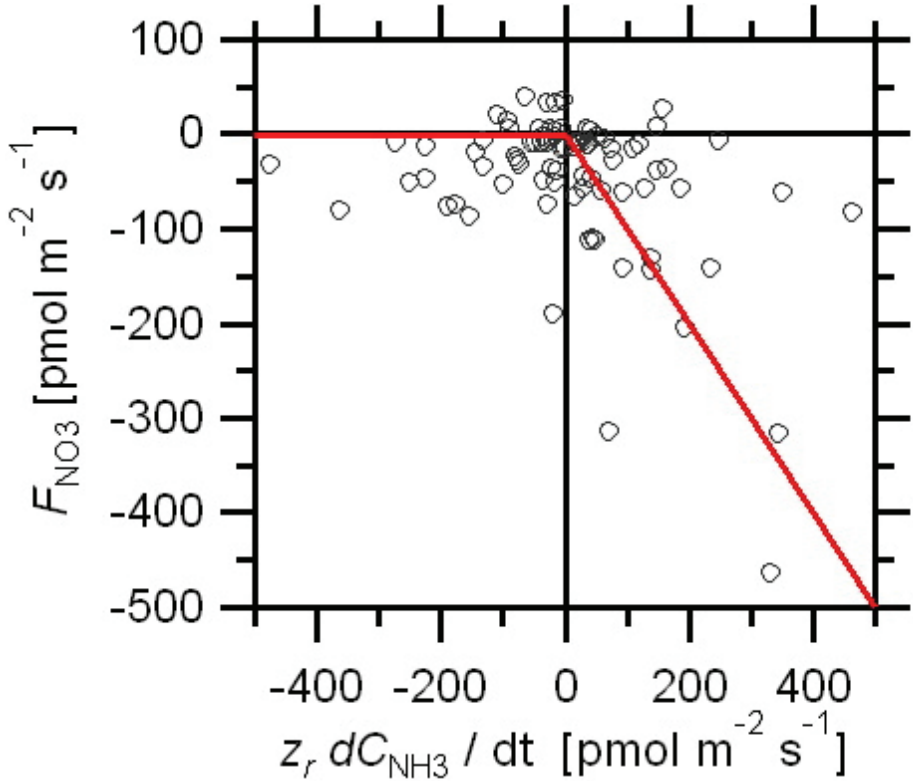

Fig. 14. Change in ammonia gas concentration compared to nitrate flux. Equation (12), representing the chemical balance if the NH_3 increase is strictly due to NH_4NO_3 evaporation, is shown in red.

ACPD
10, 22469–22513, 2010

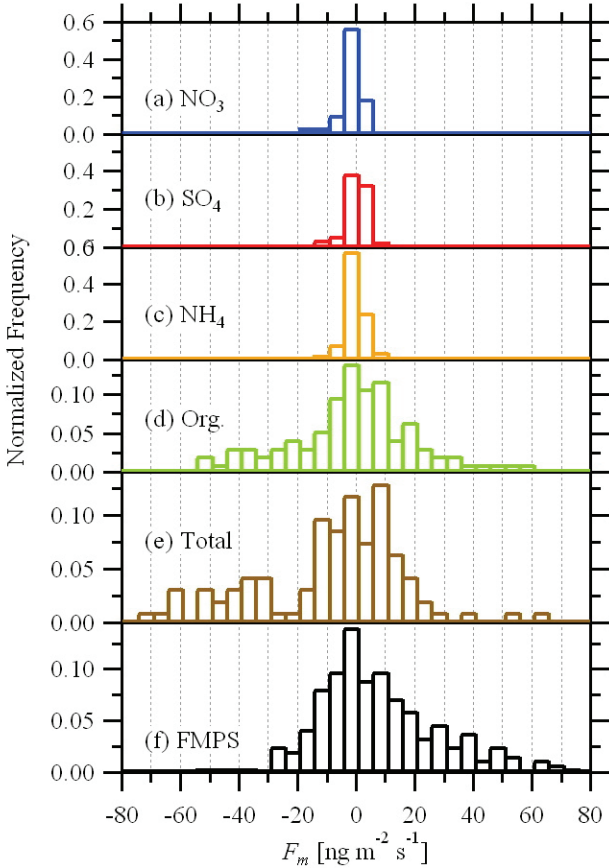

Fig. 15. A comparison of the distributions of mass fluxes (normalized by the total number of observations) from both studies, for: individual chemical species from the 2006 Q-AMS measurements of nitrate **(a)**, sulphate **(b)**, and organics derived from m/z=43 **(c)**; total mass flux from the Q-AMS **(e)**; and total mass flux from the FMPS in 2009 for the equivalent size range **(f)**.

ACPD
10, 22469–22513, 2010